Pool boiling heat transfer on artificial micro-cavity surfaces in dielectric fluid FC-72

2006 J. Micromech. Microeng. 16 2092

(http://iopscience.iop.org/0960-1317/16/10/024)

INSTITUTE OF PHYSICS PUBLISHING JOURNAL OF MICROMECHANICS AND MICROENGINEERING

J. Micromech. Microeng. **16** (2006) 2092–2099 doi:10.1088/0960-1317/16/10/024

Pool boiling heat transfer on artificial micro-cavity surfaces in dielectric fluid FC-72

Chih Kuang Yu[1], Ding Chong Lu[1] and Tsung Chieh Cheng[2]

[1] Department of Mechanical Engineering, National Chiao Tung University, Hsin-Chu, Taiwan
[2] Nanometrology, National Nano Device Laboratories, Hsin-Chu, Taiwan

E-mail: tccheng@mail.ndl.org.tw and ivanckyu@itri.org.tw

Received 25 February 2006, in final form 30 July 2006
Published 29 August 2006
Online at stacks.iop.org/JMM/16/2092

Abstract

The boiling performance and flow mechanism on artificial micro-cavity surfaces with different geometric parameters are presented in the present study. The test surfaces are manufactured on a 625 μm thick, 10 mm $\times$ 10 mm square silicon plate. The treated cavities are all cylinders with three diameters (200, 100 and 50 μm) and two depths (200 and 110 μm). The densities of the cavities were designed to be 33 $\times$ 33, 25 $\times$ 25 and 16 $\times$ 16 arrays with 100, 200 and 400 μm spacings, respectively. The characteristics of heat transfer for pool boiling of FC-72 on artificial micro-cavity surfaces were also examined. In this paper, visualization of the flow patterns was conducted to investigate the characteristics of the bubbles in the growth and departure process. The results indicated that boiling incipience and temperature excursion of silicon-based surfaces are more significant than those of metal-based surfaces reported in the literature. The effects of cavity density are stronger in the high heat flux region than in the low heat flux region because of the bubble/vapor coalescence near the heating surface. The heat transfer coefficient increases with heat flux and cavity density but a denser cavity will suppress the value of critical heat flux (CHF). Besides, in moderate and high heat flux regions, a larger cavity diameter surface shows earlier decay and a lower peak value of the heat transfer coefficient. The maximum value of CHF on the base area was 3×10^5 W m^{-2} (30 W m^{-2}) for the test surface with a 33 $\times$ 33 cavity array, which is almost 2.5 times that of the plain silicon surface.

1. Introduction

Direct immersion cooling in a dielectric liquid with a phase change is a good method for removing the large amount of heat generated from high power density devices. There are several parameters which can be used to improve the pool boiling heat transfer performance, such as pressure, sub-cooling, dissolved gas content, orientation and surface structure. Zhang and Shoji [1] studied the physical mechanisms of nucleate site interaction in pool boiling and found that there are three crucial effect factors—hydrodynamic interaction between bubbles, thermal interaction between nucleate sites, horizontal and declining bubble coalescences. Besides, a single artificial cavity was analyzed through the nonlinear behavior method and low-dimensional chaos of the bubbles [2, 3]. Recently, Honda [4] observed that a silicon chip with the micro-pin-fin in FC-72 revealed a considerable heat transfer enhancement.

The pool boiling mechanism is very complex with several factors considering high heat transfer rates including the latent heat transfer, natural convection and micro-convection. Several investigators used visualization as a tool to quantify the relative contribution of the above-mentioned components. Nakayama *et al* [5–8] were among the first to carry out visualization of the boiling process from a structured surface. The surface consisted of a rectangular channel covered with a thin sheet with pores at a regular pitch and the entire structure was immersed in R-11. Arshad and Thome [9] conducted visualization from similar surfaces to understand

the mechanism of boiling inside the channels. Xia *et al* [10] observed that the boiling hysteresis attenuates as narrow channels and the first local bubble site is active on the upper part of the narrow channel. An infrared radiator image system and an optical system combining a microscope and a high-speed camera were used by Xu *et al* [11, 12] to observe transient flow pattern identification in microchannels. Besides, the forced convection boiling in microchannels was observed by Lee *et al* [13] to monitor the bubble activity.

Boiling is a high-efficiency heat transfer technique in many application fields. Both pool boiling and flow boiling are restricted in the nucleate boiling region by two factors: boiling hysteresis and critical heat flux (CHF). Therefore, how to reduce the boiling incipience temperature and increase the CHF value is an important issue for extending the limitation of boiling heat transfer technology in the electronic cooling application. In this paper, a series of pool boiling experiments were established and employed to investigate the boiling heat transfer performance including the boiling incipience, heat transfer coefficient and critical heat flux on artificial micro-cavity surfaces immersed in the dielectric fluid with various geometry parameters. Moreover, the direct visual observation was also used to investigate the flow patterns of those surfaces for understanding the boiling heat transfer mechanism of the microstructure.

2. Experimental apparatus

A test module immersed inside a hermetic stainless steel pressure chamber with 304 mm height and 154 mm diameter, as shown in figure 1, was used to simulate the boiling phenomenon in the saturated dielectric liquid FC-72 at atmospheric pressure. The internal water condenser was coiled inside the chamber and connected with a thermostat to maintain the chamber at atmospheric pressure. A pressure transducer with operating range of 0–400 kPa was also located at the gate of the chamber to measure the pressure. The liquid temperature was measured by two resistance temperature detectors (RTDs) with the calibrated accuracy of 0.1 K. In order to protect against the heat loss from the vessel to the ambient, an auxiliary cartridge heater was wrapped around the chamber to maintain the liquid temperature during the experiment. The heating module consists of four major parts: test surface, dummy heater, Bakelite frame insulator and Teflon substrate insulator. A thin heater (0.1 mm thickness) with an electrical resistance of about 10 Ω was also attached to the Teflon substrate ($k \approx 0.35$ W m^{-1} K^{-1}) to reduce the heat loss. The power generated from the dummy heater was provided by a dc power supply (0–160 V, 0–5 A). The signals, detected from thermocouples, RTDs and the pressure transducer were all collected and converted by the internal calibration equation during the data acquisition, and then the converted signals were transmitted through the GPIP interface to a personal computer. In addition, a microscope–high-speed camera system (Fuji S602) was installed in front of the quartz window to observe the mechanism of boiling from these micro-cavity surfaces and the boiling images were also stored and displayed by a PC through the image-capturing software.

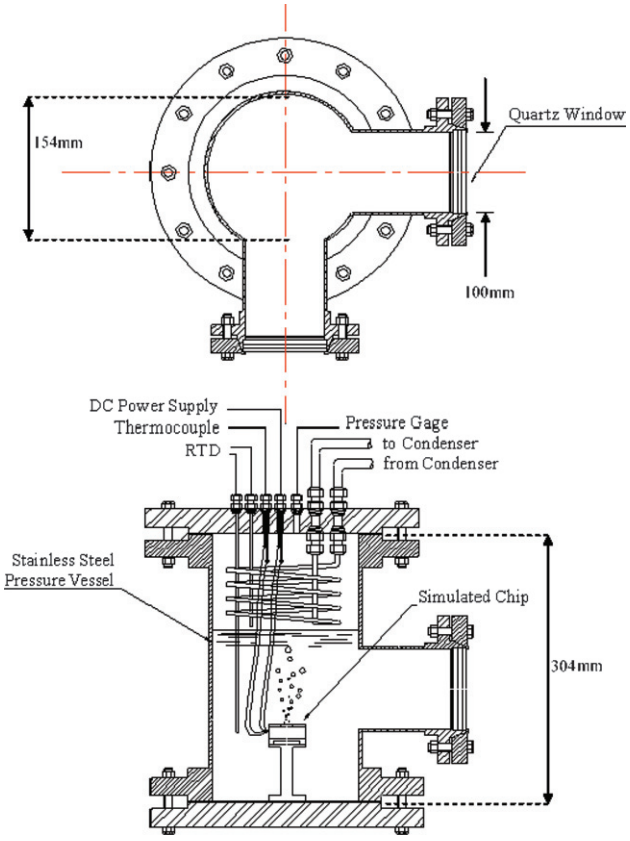

Figure 1. Schematic of the pool boiling test apparatus.

3. The fabrication of artificial micro-cavity surfaces

Microfabrication is a process of etching, patterning and layering materials into microstructures. Bulk micromachining, which was used to fabricate some mechanical structures and create within the confines of a silicon wafer by selectively removing parts of the wafer material device, is a widely used technology for making MEMS devices. Through bulk micromachining, the etching process can be either isotropic, anisotropic or a combination of both. In isotropic etching, the etch rate is identical in all directions, while in anisotropic etching the etch rate depends on the crystallographic orientation of the wafer [14].

The micro-cavities were produced by some simple processes as shown in figure 2. The 3D artificial micro-cavities can be formed through the two-mask process. In order to avoid distortion and bending of silicon because of the thermal expansion effect, the stage is required to provide a fixed contact and a small gap. The microfabrication process, as illustrated in figures 2(*a*)–(*c*), started with a dummy (1 0 0) double-side polished silicon wafer and the positive resist AZ6420 was used for stage patterning. Then Oxford ICP dry etching was used to make a vertical sidewall. In addition, the silicon nitride (Si_3N_4) was grown by the LPCVD technique and used for the etching barrier to resist Oxford ICP dry anisotropic etching. Finally, after removing the silicon nitride by RIE dry etching, the micro-cavity structure can be formed and the depth of artificial micro-cavities can easily be controlled by the etching time of Oxford ICP dry anisotropic etching. SEM pictures

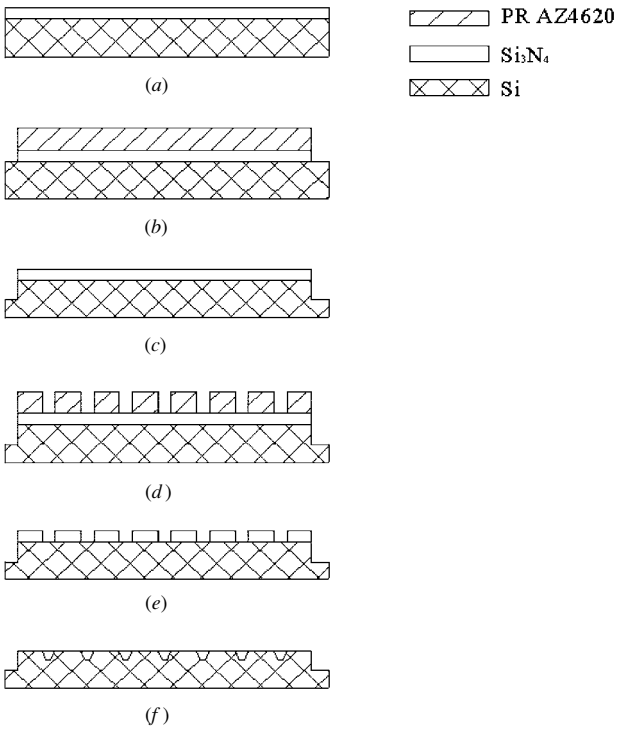

Figure 2. The process flow of a test artificial micro-cavity surface.

of a test artificial micro-cavity surface are also presented in figure 3.

4. Data reduction

For analyzing the boiling heat transfer performance, the overall heat transfer coefficient of rectangular fin array is defined as

$$h_t = q''_{total}/\Delta T, \tag{1}$$

where q''_{total} is the heat flux based on the total area and ΔT is the wall superheat which can be calculated from the experimental measurement. The heat transfer rate $\dot{Q}$ can be obtained from the voltage and current through the dc power supply. The heat fluxes (q''_b and q''_t) which depend on the base surface area (A_b) and total surface area (A_t, equal to the sum of the base area and cavity area) are summarized as follows:

$$\dot{Q} = I \times V, \tag{2}$$

$$q''_b = \dot{Q}/A_b, \tag{3}$$

$$A_b = (L)^2, \tag{4}$$

$$q''_t = \dot{Q}/A_t, \tag{5}$$

$$A_t = A_b + n\left(\pi d_c H_c + \frac{\pi d_c^2}{4}\right), \tag{6}$$

where d_c and H_c are the diameter and depth of the cavity, respectively.

Then the heat transfer inside the base of a fin array can be obtained from the one-dimensional heat conduction:

$$T_b = T_m - q''_b \Delta x/k, \tag{7}$$

where T_m is the average value of temperature measurement, Δx is the thickness of the test surface and k is the thermal conductivity of silicon. The wall superheat (ΔT) is defined as the difference between the temperature of base surface (T_b) and the saturated temperature of FC-72 (T_{sat}).

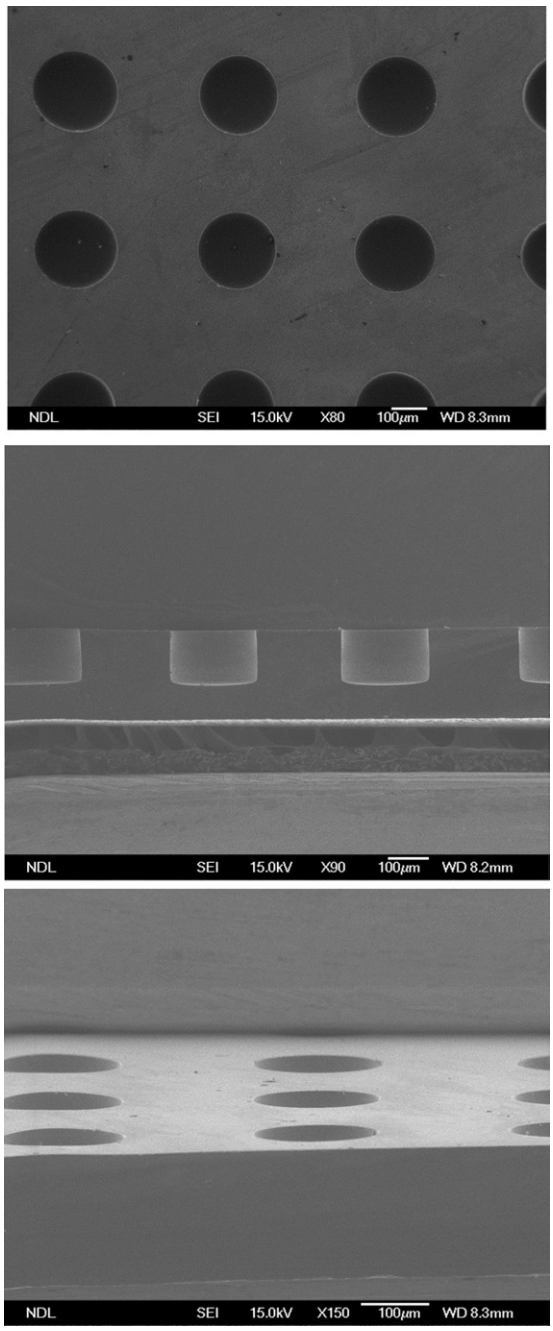

Figure 3. SEM pictures of a test artificial micro-cavity surface (25 × 25 array, cavity diameter 200 μm, depth 110 μm).

In fact, the insulators of the heating module including the Bakelite frame and Teflon substrate cannot absolutely prevent the heat loss. In order to understand the influences of this heat loss effect, the commercial computation fluid dynamic software Flotherm was used to estimate the heat loss. The results indicated that the heat loss with the heat flux from 0.2 W to 1 W was 15.5% to 9.3%. Hence, the heat losses can be neglected in our experiment.

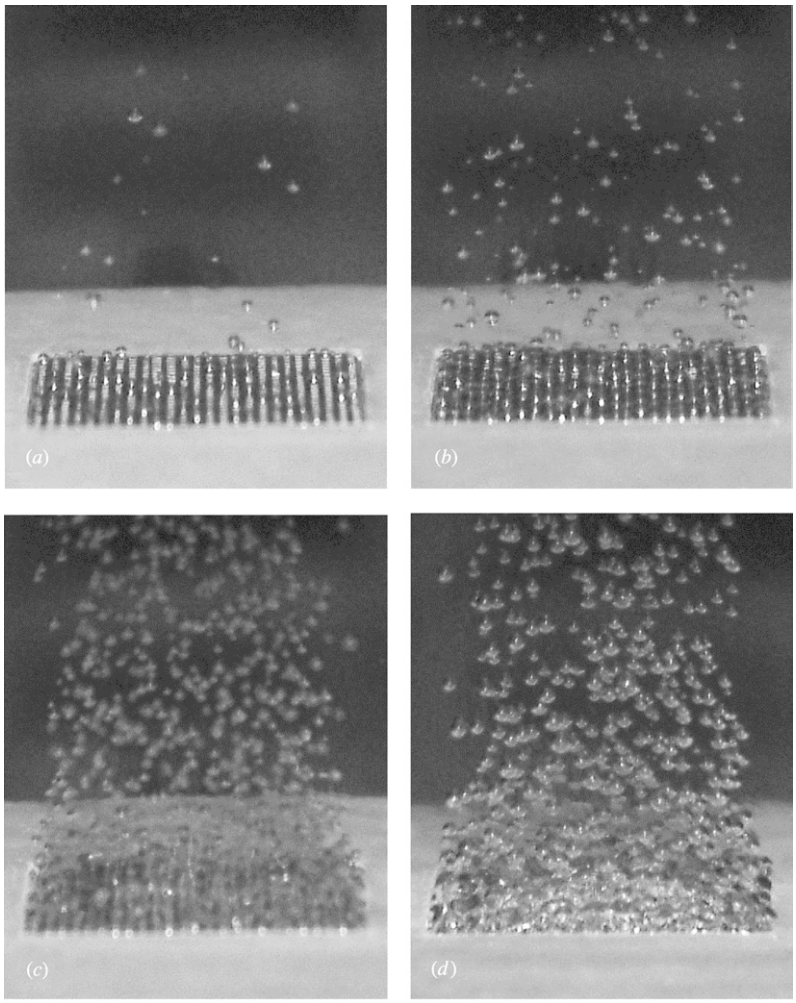

Figure 4. Flow patterns of a micro-cavity surface with cavity density of 25 × 25: (*a*) 11.7% of CHF; (*b*) 28.4% of CHF; (*c*) 56.5% of CHF; (*d*) 78.6% of CHF.

Table 1. Uncertainty analysis of the experiments.

Parameter	Uncertainty
Test surface geometry	
Width of plain surface (%)	±0.5
Area of cavity surface (%)	±1.0
Cavity diameter and depth (%)	±0.5
Area of cavity surface (%)	±4.0
Parameter measurement	
Temperature, T (°C)	±0.2
Temperature difference, ΔT (°C)	±0.4
System pressure, P (kPa)	±0.5
Boiling heat transfer on plain surface	
Power input, $\dot{Q}$ (%)	±9.2
Heat flux, q'' (%)	±11.8
Heat transfer coefficient, h (%)	±13.4
Boiling heat transfer on finned surface	
Power input, $\dot{Q}$ (%)	±9.2
Heat flux, q'' (%)	±14.2
Heat transfer coefficient, h (%)	±16.4

Uncertainty analysis such as heat flux and temperature measurements was analyzed by the procedures proposed by Kline and McClintock [15]. The detailed results from the present uncertainty analysis are summarized in table 1.

5. Results and discussion

5.1. Flow pattern observation of micro-cavity surfaces

In order to understand the characteristics of saturated FC-72 boiling on micro-cavity surfaces, photos taken for the case with different cavity densities are shown in figures 4 and 5. A closed inspection of the photo in figure 4 indicates that at boiling incipience the bubble population is less but uniformly and randomly generated from the cavities. Bubble birth and departure seems to be periodic, and shapes of bubbles are almost perfectly spherical. Besides, the observed bubbles that depart from cavities are small and discrete without any interaction or coalescence. For a little rise in the heat flux values, as shown in figures 4(*a*) and 5(*a*), the number of active cavities and bubble departure frequency observably increased. Higher departure frequency also results in vertical coalescence above some cavities after bubbles leaving the cavities. At a moderate heat flux, as shown in figures 4(*b*) and 5(*b*), some growing bubbles begin to coalesce horizontally with each other in adjacent cavities, so the cavity surface was covered with coalesced bubbles and some vapor columns were also formed. Obviously, horizontally coalesced bubbles result in larger flow resistance to obstruct the rewetting liquid entering the cavities

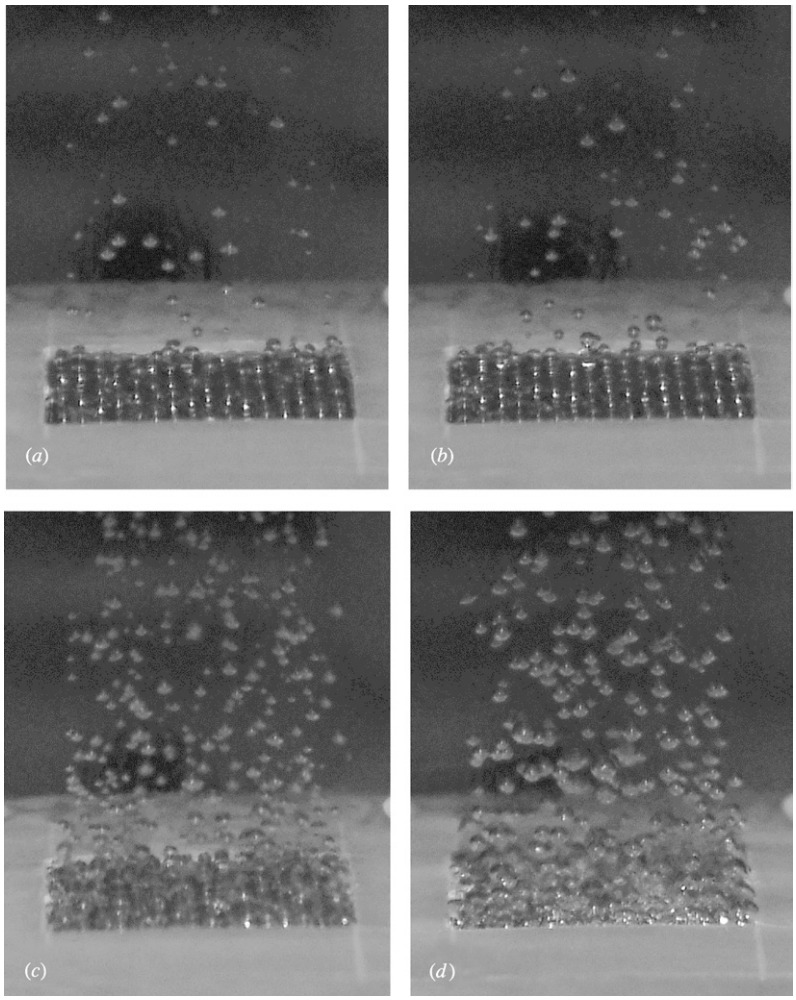

Figure 5. Flow patterns of a micro-cavity surface with cavity density of 16 × 16: (*a*) 14.8% of CHF; (*b*) 33.9% of CHF; (*c*) 55.1% of CHF; (*d*) 75.9% of CHF.

and also delayed the bubbles/vapor departure time at the same time. Moreover, the larger deformed bubbles or some vapor mushrooms are observed due to the horizontal bubble/vapor coalescence. Finally, at extremely high heat flux, as shown in figures 4(*d*) and 5(*d*), it is clearly observed that large vapor mushroom clouds blanket the entire cavity surface. Even as the heat flux approaches CHF, the vapor mushroom clouds result in some columns like a twisted column filled with large bubbles. Apparently, this twist phenomenon would cause the exhaustion of rewetting liquid and result in the dry-out situation near the center of the test surface and inside cavities.

6. The effects of cavity density on boiling heat transfer performance

The heat flux plotted against the wall superheat for both single-phase natural convection and nucleate boiling regime on three cavity surfaces with different cavity densities is shown in figure 6. The experimental data show that the effect of microsurface treatment, during the natural convection regime, is the slight decrease of the wall superheat with the cavity density that is presented in figure 6. For all test surfaces, boiling generally initiated a discontinuous shift of the boiling curve. The wall superheat decreases suddenly because the bubble absorbs a large amount of heat as the dielectric liquid boils. In addition, it is clearly observed that the extremely high wall superheat of the plain silicon surface (45.9 °C) is because of least nucleate sites on its highly polished surface. By contrast, the reduction of boiling incipience temperature and excursions of micro-cavity surfaces is also investigated in figure 6. In the nucleate boiling regime, the wall superheat of the cavity surface is significantly lower than that of the plain surface because of more nucleate sites on the micro-cavity surface. The results indicated that the boiling performance of the micro-cavity surface is better than that of the plain arrangement. The plots also show that at an identical heat flux, the wall superheat is low for the denser cavity surface. The smaller wall superheat, for the same heat flux, shows a better heat transfer condition for the denser cavity surface than that for the rarer surface, confirming the boiling enhancement in the low heat flux region of the nucleate regime. For the same test surface, it is investigated that the wall superheat increases with the heat flux. Moreover, with increasing heat flux, the wall superheat is higher until it becomes infinitely large at CHF. The plots in figure 6 also show that a noticeable enhancement in the CHF value of all micro-cavity surfaces is

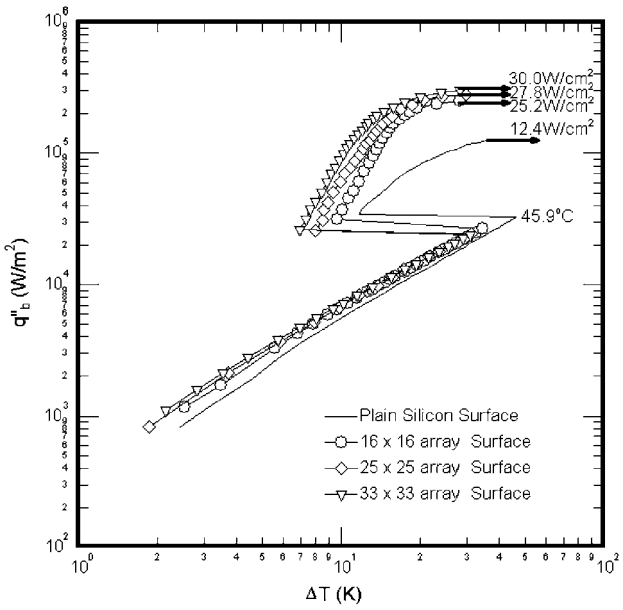

Figure 6. Boiling curves of a micro-cavity surface (cavity diameter 200 μm, depth 110 μm).

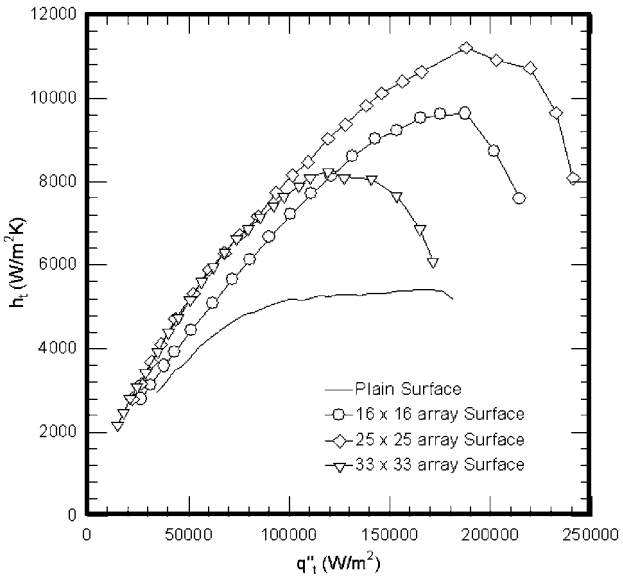

Figure 7. Variations of pool boiling heat transfer coefficient with heat flux for various cavity densities under 1 atm saturated conditions (decreasing heat flux).

due to the increase in nucleate sites. For the 33 × 33 array surface, the CHF value (30 W) is almost 2.5 times that of the plain silicon surface.

The heat transfer coefficients of the test surfaces which show the same trend with heat flux plotted versus heat flux are shown in figure 7. On increasing the heat flux, the cavity surfaces will reach a maximum value and then decrease with the increase in the heat flux. The peak of the slope is at about 180 000 W m^{-2} (18 W cm^{-2}) for 16 × 16 and 25 × 25 cavity array surfaces and 120 000 W m^{-2} (12 W cm^{-2}) for the 33 × 33 cavity array surface. This behavior with the maximum value can be explained by the fact that the active nucleate density

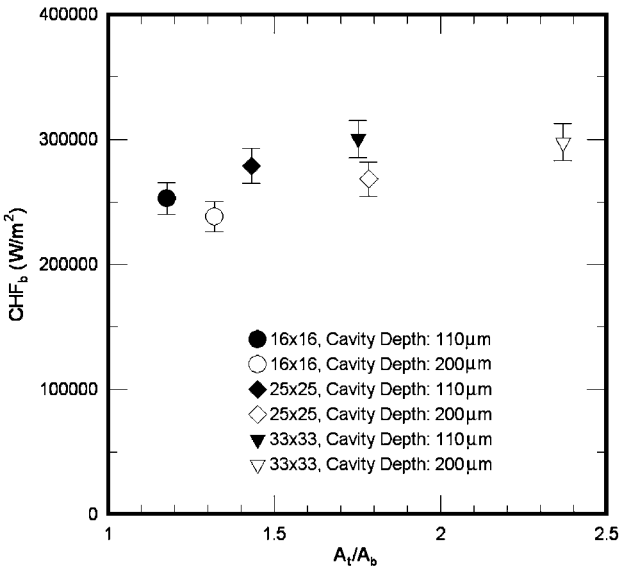

Figure 8. Variations of critical heat flux with enhancement of the area at depths 110 and 200 μm.

increases as the wall temperature rises until large clusters and horizontal accumulations of vapor are formed near the heating surface. After this peak value, the heat transfer coefficients begin to decay. This decline behavior is induced by two kinds of liquid/vapor exchange mechanisms: temporal dry-out situation inside the cylindrical cavities and vapor film blanketing the heating surface. Temporal dry-out situation is the result of the flow resistance that is induced by the cavity structure with vapor trapped in cavity impeding rewetting fluid flow into the cavity. Moreover, vapor coalescence among the adjacent cavities forms the vapor film that covers the heating surface and results in worse heat transfer efficiency due to the low thermal conductivity of vapor.

The effect of density of cavities on CHF value variations for six test surfaces is shown in figure 8. The micro-cavity surfaces consistently enhance the CHF value over the plain silicon surface. This enhancement is evidently observed in the results of the cavity surfaces. However, this enhancement mechanism seems to reach a critical value with more cavity arrays because of denser cavities which result in the horizontal coalescence and form the vapor film that covers the test surface in the high heat flux region. It is implied that the CHF values cannot always be increased with the number of cavities.

6.1. Effects of cavity diameter and depth on boiling heat transfer performance

The boiling performances of the micro-cavity surfaces that varied with the cavity diameter are also plotted in figure 9 under decreasing heat flux conditions. The cavity density is of 25 × 25 array, with 110 μm depth, and the diameter is varied from 50 to 200 μm. From the results of figure 9, one can see that the slope of the boiling curves is roughly the same regardless of the cavity diameter. It indicates that the influence of the cavity diameter on heat transfer coefficients can be

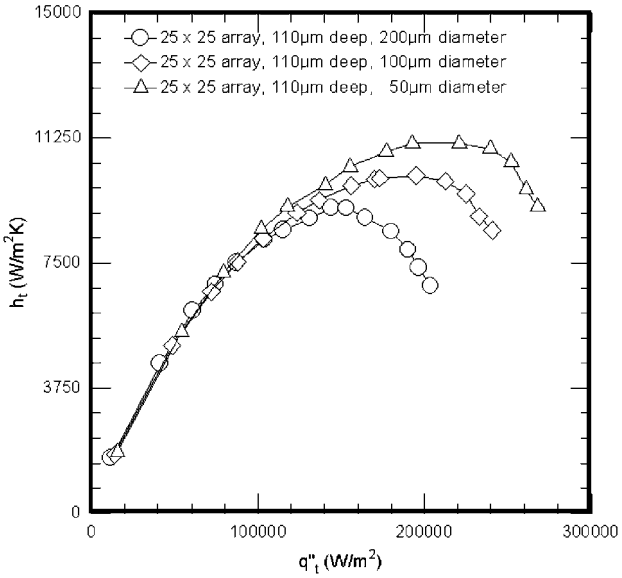

Figure 9. Variations of pool boiling heat transfer coefficient with heat flux for various cavity diameters under 1 atm saturated conditions (decreasing heat flux).

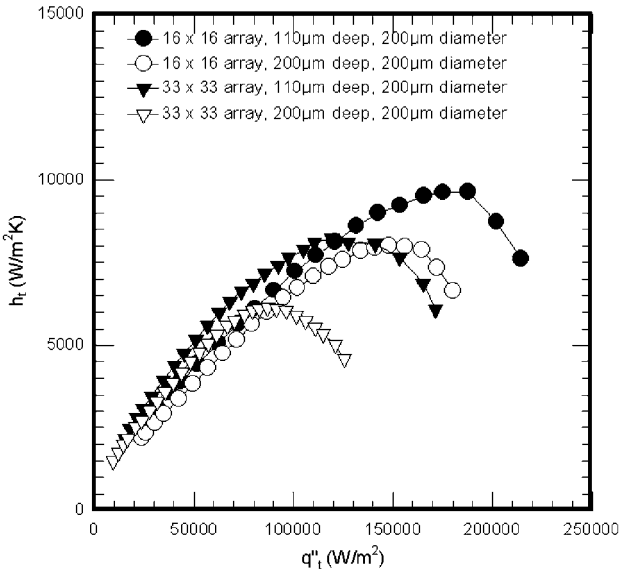

Figure 10. Variations of pool boiling heat transfer coefficient with heat flux for various cavity depths under 1 atm saturated conditions (decreasing heat flux).

ignored as the inferior heat flux region is below 80 000 W m^{-2} (8 W cm^{-2}). The same trends were also observed by Shoji *et al* [2]. However, earlier decay and lower peak value of the boiling heat transfer coefficient for a larger cavity diameter surface are observed in moderate and high heat flux regions. The flow pattern shows that departure bubble diameter increases with cavity diameter and growing bubbles of larger diameter cavity easily coalesce with adjacent bubbles due to smaller cavity spacing. This bubble interaction manifests that horizontal coalescence results in lower heat transfer performance in moderate and high heat flux regions.

Finally, the effects of the cavity depth on the overall boiling heat transfer coefficient are also examined in figure 10. The figure presents the behaviors of the overall heat transfer coefficients on micro-cavity surfaces with cavity densities of 33 × 33 and 16 × 16 and cavity depths of 200 and 110 μm. Note the premature rapid decline of overall heat transfer coefficients for deeper cavities. In the nucleate boiling region, the hydrodynamic interaction which is the vapor/liquid exchange mechanism can be influenced by the cavity depth. Deeper cavities pull the departure bubble and decrease the bubble departure frequency. It is indicated that the bubble pulled by hydrodynamic interactions and the residual vapor will be trapped inside the cavity. This will produce the flow resistance to obstruct the rewetting liquid entering the cavities.

7. Conclusions

An experimental study on the saturated boiling of FC-72 with different artificial micro-cavity surfaces is examined in this paper. The pool boiling heat transfer performances and flow patterns of these cavity surfaces were also obtained in the saturated dielectric fluid FC-72 at atmospheric pressure. The major results can be briefly summarized as follows:

(1) The effect of cavity density is stronger in the high heat flux region than in the low heat flux region because of the horizontal bubble/vapor coalescence near the heating surface. The critical heat flux is dependent on the cavity density and the CHF enhancement is almost proportional to the area enhancement of the cavity surface. Besides, the heat transfer coefficient of test surfaces increases with heat flux and cavity density but the value of CHF will be suppressed by denser cavities.

(2) The influence of the cavity diameter on heat transfer coefficients in the inferior heat flux region below 80 000 W m^{-2} (8 W cm^{-2}) can be ignored. In moderate and high heat flux regions, a larger cavity diameter surface would induce earlier decay and lower peak value of the boiling heat transfer coefficient.

(3) Increasing the depth of cavities will result in premature rapid decline of overall heat transfer coefficients, which due to the larger flow resistance of deeper cavities obstruct the rewetting liquid entering these cavities.

(4) The maximum value of CHF on the base area was 3 × 10^5 W m^{-2} (30 W cm^{-2}) for the test surface with a 33 × 33 cavity array, which is almost 2.5 times that of the plain silicon surface.

References

[1] Zhang L and Shoji M 2003 Nucleate site interaction in pool boiling on the artificial surface *Int. J. Heat Mass Transfer* **46** 513–22

[2] Shoji M and Takagi Y 2001 Bubbling features from a single artificial cavity *Int. J. Heat Mass Transfer* **44** 2763–76

[3] Chatpun S, Watanabe M and Shoji M 2004 Experimental study on characteristics of nucleate pool boiling by the effects of cavity arrangement *Exp. Therm. Fluid Sci.* **29** 33–40

[4] Honda H and Wei J J 2003 Effects of fin geometry on boiling heat transfer from silicon chips with micro-pin-fins immersed in FC-72 *Int. J. Heat Mass Transfer* **46** 4059–70

[5] Nakayama W, Daikoku T, Kuwahara H and Nakajima T 1980 Dynamic model of enhanced boiling heat transfer on porous surfaces: part I. Experimental investigation *J. Heat Transfer* **102** 445–50

[6] Nakayama W, Daikoku T, Kuwahara H and Nakajima T 1980 Dynamic model of enhanced boiling heat transfer on porous surfaces: part II. Analytical modeling *J. Heat Transfer* **102** 451–6

[7] Nakayama W, Daikoku T and Nakajima T 1982 Effects of pore diameters and system pressure on saturated pool boiling heat transfer from porous surfaces *J. Heat Transfer* **104** 286–91

[8] Ramaswamy C, Joshi Y, Nakayama W and Johnson W B 2002 High-speed visualization of boiling from an enhanced structure *Int. J. Heat Mass Transfer* **45** 4761–71

[9] Arshad J and Thome J R 1983 Enhanced boiling surfaces: heat transfer mechanism and mixture boiling *Proc. ASME–JSME Thermal Engineering Joint Conf.* vol 1 pp 191–7

[10] Xia C, Hu W and Guo Z 1996 Natural convective boiling in vertical rectangular narrow channels *Exp. Therm. Fluid Sci.* **12** 313–24

[11] Xu J, Gan Y, Zhang D and Li X 2005 Microscale boiling heat transfer in a micro-timescale at high heat fluxes *J. Micromech. Microeng.* **15** 1344–61

[12] Xu J, Shen S, Gan Y, Li Y, Zhang W and Su Q 2005 Transient flow pattern based microscale boiling heat transfer mechanisms *J. Micromech. Microeng.* **15** 362–76

[13] Lee M, Cheung L S L, Lee Y K and Zohar Y 2005 Height effect on nucleation-site activity and size-dependent bubble dynamics in microchannel convective boiling *J. Micromech. Microeng.* **15** 2121–29

[14] Ristic L 1994 *Sensor Technology and Devices* (Boston, MA: Artech House) chapter 3, pp 50–76

[15] Kline S J and McClintock F A 1953 Describing the uncertainties in single-sample experiment *Mech. Eng.* **75** 3–8